ACS APPLIED MATERIALS & INTERFACES



Article

# Integration of a Genetically Encoded Calcium Molecular Sensor into Photopolymerizable Hydrogels for Microoptrode-Based Sensing

Leyla Nesrin Kahyaoglu, Rajtarun Madangopal, Joon Park, and Jenna L. Rickus

*ACS Appl. Mater. Interfaces*, **Just Accepted Manuscript** • DOI: 10.1021/acsami.7b09923 • Publication Date (Web): 28 Aug 2017



## Just Accepted



ACS Publications

ACS Applied Materials & Interfaces is published by the American Chemical Society.
1155 Sixteenth Street N.W., Washington, DC 20036

# Integration of a Genetically Encoded Calcium Molecular Sensor into Photopolymerizable Hydrogels for Microoptrode-Based Sensing

Leyla Nesrin Kahyaoglu[a,c], [†]Rajtarun Madangopal[b,c], Joon Park[a,c], Jenna L. Rickus*[a,b,c]

[a] Agricultural & Biological Engineering; [b] Weldon School of Biomedical Engineering;

[c]Birck-Bindley Physiological Sensing Facility,

Purdue University, West Lafayette, Indiana, USA.

KEYWORDS: genetically encoded protein biosensor, optrode, photocurable hydrogel, optical biosensor, GCaMP, calcium sensing, photopolymerization

ABSTRACT: Genetically encoded molecular protein sensors (GEMS) are engineered to sense and quantify a wide range of biological substances and events in cells, *in vitro* and even *in vivo* with high spatial and temporal resolution. Here, we aim to stably incorporate these proteins into a photopatternable matrix, while preserving their functionality, to extend the application of these proteins as spatially addressable optical biosensors. For this reason, we examined the fabrication

of 3D hydrogel microtips doped with a genetically encoded fluorescent biosensor, GCaMP3, at the end of an optical fiber. Stable incorporation parameters of GCaMP3 into a photocrosslinkable monomer matrix were investigated through a series of characterization and optimization experiments. Different precursor solution formulations, and irradiation parameters of *in situ* photopolymerization were tested to determine the factors affecting protein stability and sensor reproducibility during photoencapsulation. Microstructure and performance of hydrogel microtips were controlled by varying UV irradiation intensity as well as photocurable monomer, PEGDA (polyethylene glycol diacrylate) molecular weight and concentration in precursor solution. Protein doped hydrogel microoptrodes (microtip sensors) were fabricated successfully and reproducibly at the distal end of optical fiber. Under optimized conditions, bioactivity of GCaMP3 within hydrogel matrix of microoptrodes remained similar to that of protein free in buffer. The limit of detection of protein optrodes for free calcium was also determined to be 4.3 nM. The hydrogel formulation and fabrication process demonstrated here using microtip optrodes can be easily adapted to other conformation-dependent protein biosensors and be used in sensing applications.

## 1. INTRODUCTION

The scope of possible optical biosensors is restricted by available analyte-sensitive dyes or molecular sensors. In recent years, protein engineering has produced several families of novel genetically encoded molecular sensors (GEMS), which are typically synthetic fusion proteins containing an analyte-binding region and at least one fluorescent sensor region[1-3]. GEMS were developed and used primarily for the imaging of metabolites and signaling molecules in tissues, transgenic animals or in roots of intact plants by expressing the GEMS in the subject organism as

a transgene[2,4,5]. However, these protein-based sensor molecules also open up opportunities to create new optical biosensor devices including optical sensors or optrodes. Optrodes compliment imaging as a sensing tool particularly in applications where the genetic manipulation of the subject organism is not desirable or practical, such as implantable devices in humans and environmental monitoring.

To build an optrode using a GEMS, the synthetic protein must interface with an optical component such as an optical fiber or waveguide. Recently, studies demonstrated the covalent immobilization of GEMS proteins on the surface of silica nanoparticles [6] and the incorporation of GEMS proteins within silica nanoparticles through specific interaction between histidine residues of protein and calcium–silicate complex of the silica matrix[7]. In general, the immobilization or encapsulation of proteins into 3D matrices results in better protein stability and function compared to covalent modification or adsorption to flat planar surfaces[8]. Photocrosslinkable hydrogels offer not only a highly hydrophilic 3D environment to foster protein activity and stability, but are also optically addressable to enable spatially controlled protein localization[9-11]. The photoencapsulation of GEMS has not been reported up to date. This lag could be attributed to fragile nature of these proteins, which might need special requirements to be encapsulated properly.

In this work, our goal was to develop a universal and facile physical entrapment method for the immobilization of genetically encoded protein biosensors into a spatially patternable, 3D hydrogel matrix. To meet this goal the matrix material must i) allow the molecular structure and movement of the sensor protein required for signal transduction, ii) be porous enough to allow good diffusional exchange with the surrounding fluid, iii) be optically transparent, and iv) be able to be grown, printed or deposited on optical components for device integration. To fulfill

these four criteria, we selected water-soluble and photocrosslinkable, polyethylene glycol diacrylate (PEGDA) as a precursor to fabricate our protein encapsulation matrix. The diacrylate moieties provide a means to control the polymerization via photocrosslinking and the PEG moieties offer stealth and volume exclusion effects that can effectively stabilize the protein and reduce steric constraints while retaining bioactivity[12,13].

We chose the engineered protein, GCaMP3, as a model sensor protein. The GCaMPs are a family of single-fluorescence genetically encoded calcium indicators (GECIs) that have been extensively characterized and used for *in vivo* calcium imaging across multiple model organisms[2,14,15]. GCaMP3 consists of a circularly permuted enhanced green fluorescence protein (EGFP, Ex/Em 488 nm/512 nm) flanked between the calcium binding protein, calmodulin, and the calmodulin binding peptide M13 (Fig. 1a). When exposed to calcium, the interaction of calmodulin with M13 induces changes in the fluorophore environment leading to an increase in the emitted fluorescence[2] (Fig. 1a). The GCaMPs have been primarily expressed in brain tissue to image neuronal network activity and have therefore been optimized for this purpose. Because the local environment influences the signal output and because ligand-induced conformational changes are necessary for sensor function, the translation of GCaMP from cellular to a synthetic polymeric environment with different polarity and limited molecule flexibility may have an impact on protein response, bioactivity, and stability. For this reason, we first investigated the effect of the photopolymerization conditions and polymer matrix properties on GCaMP3 function. We then optimized these parameters based on sensor performance and demonstrated the use of this matrix system to build a GEMS based calcium micro-optrode.

## 2. EXPERIMENTAL SECTION

2.1. Chemicals and materials

$PEG_{300}DA$ ($M_n$ 300 Da), $PEG_{500}DA$ ($M_n$ 500 Da), and $PEG_{740}DA$ ($M_n$ 740 Da) were received as a gift from Sartomer Company, Inc. (Exton, PA). $PEG_{3400}DA$ (Mn 3400 Da) was purchased from Alfa Aesar (Ward Hill, MA). All monomers were used as received. The photoinitiator, 1-[4-(2-Hydroxyethoxy)-phenyl]-2-hydroxy-2-methyl-1-propane-1-one, IR2959 was a kind gift from Ciba Specialty Chemicals.

2.2. Protein expression, purification and characterization

The calcium binding protein (GCaMP3) was expressed and purified using a previously published protocol[2]. Protein concentration was determined by using a Nanodrop ND-1000 Spectrophotometer. Calcium calibration buffers were made with 10 mM blends of CaEGTA and $K_2EGTA$ in 30 mM MOPS and 100 mM KCl;KOH at pH 7.4[16]. Free [$Ca^{2+}$] levels were calculated using Maxchelator[17]. Fluorescence spectra ($\lambda_{ex,peak}$ = 470nm, $\lambda_{em,peak}$ = 512 nm) were recorded using a SpectraMax M5 fluorescent plate reader (Molecular Devices). The fluorescence emission was normalized according to the equation: $(F-F_{min})/(F_{max}-F)$. F is the fluorescence emission intensity at any calcium concentration. $F_{max}$ is the fluorescence emission intensity at saturating 39 μM [$Ca^{2+}$], and $F_{min}$ is the fluorescence intensity at zero [$Ca^{2+}$].

2.3. Characterization of precursor solution

The effect of photoinitiator (1% w/w), UV exposure times (0, 10, 30, 60 and 300 seconds) and the presence of PEGDA (10% w/w $PEG_{740}DA$) on protein bioactivity was investigated. GCaMP3 biactivity test was performed in a 96-well plate. Each well with 10 μM protein (in 30 mM MOPS, 100 mM KCl;KOH at pH 7.4) was irradiated with UV light via a 1000 μm core

multimode fiber (2 W $cm^{-2}$, 325 nm Omnichrome Series 74, He/Cd gas laser) for the specified periods of time. The power density at the end of multimode optical fiber was calculated assuming a Gaussian beam profile. The dynamic range, ($F_{max}/F_{min}$), was monitored by adding calcium-saturated (39 μM free calcium) and calcium-free (0 μM) buffers to three adjacent wells for each treatment. Precursor solutions (10% w/w of $PEG_{500}DA$, $PEG_{740}DA$, $PEG_{3400}DA$ with 1% w/w IR2959) were prepared in standard 1-cm wide disposable cuvettes, and optical attenuation was calculated from optical transmission measurements obtained from Varian Cary 50 UV-VIS Spectrophotometer (Agilent).

For swelling experiments, PEG hydrogel discs were prepared by varying PEGDA molecular weights (500, 740 and 3400 Da) and concentrations (10%, 20% and 30 %w/w) with 1% w/w IR2959. To form the disks of fixed thickness, 50 uL of each hydrogel precursor solution was carefully injected between two glass plates of a custom-made glass mold (Supporting information Fig. S1) so that they formed a stable disc shaped droplet held by surface tension. The liquid discs were than crosslinked in place via exposure to UV light for an hour (CL-1000 UV crosslinker). The discs were then placed into MOPS buffer overnight, and the swollen weights were recorded the next day. Swollen discs were lyophilized to a constant weight. The swelling ratio was determined by using the following equation: swelling ratio (SR)= $(W_s-W_d)/W_d$, where $W_s$ and $W_d$ represent the mass of swollen hydrogel and the mass of dried hydrogel, respectively. Mesh sizes and crosslinking densities of hydrogel discs with different precursor compositions were estimated using Flory-Rehner model[18,19] (details of calculations are provided in Supporting information S1).

2.4. Microtip fabrication

A Helium-Cadmium (He/Cd) laser (Omnichrome Series 74) with two lines (325 nm and 442 nm) was used as the UV light source for the microtip fabrication. A short pass filter (400 nm, Edmund Optics) was used to filter out the 442 nm laser line. Neutral density (ND) filters (Edmund optics) were introduced into the setup to attenuate the laser power when necessary. The transmitted 325 nm laser line was coupled to the fiber optic patch cable through an UVFS plano convex lenses (LA4306, Thorlabs). A high-OH multimode optical fiber for 250- 1200 nm (50 μm core/125 μm cladding, 0.22 NA, Thorlabs) was used as the sensing element for microtip fabrication. For all experiments, the fiber bare end was clipped and then cleaved using FC-6S Optical Fiber Cleaver (Sumimoto Electric Lightwave). The output power of 325 nm laser line was monitored using a laser power meter (PM100A, Thorlabs) and controlled with a xyz micro positioner. The recombinant fusion protein, GCaMP3 was added to the precursor solution of PEGDA and IR2959. Protein-based precursor solution was then filled in a borosilicate glass tube and mounted on the opposite xyz manipulator (Supporting information Fig. S2). The fiber end face was aligned to the borosilicate glass tube and carefully inserted in the photopolymer solution. Microtip growth was then initiated for 10 seconds with the set laser power using a custom shutter assembly trigged by a pulse generator (BNC, Model 555) (Supporting information Video 1). The microtip sensor was rinsed first in EtOH and then in MOPS buffer repeatedly to remove excess uncured precursor solution.

2.5. Optimization and Characterization of microtip sensor

The set-up for the characterization of the resulting sensors is shown in detail in the Supporting Information Fig. S3. GCaMP3 doped sensor microtips were evaluated by measuring the fluorescence response when dipped into buffer solutions of known free calcium concentrations.

Microtips were excited using a 470 nm LED (LLS470, Ocean Optics Inc.) and fluorescence spectra were collected using a commercial fiber coupled spectrometer (QE Pro miniature fiber optic spectrometer, Ocean Optics Inc.) (Fig. 1b).

The precursor solution parameters, final protein concentration (0.5 mg/ml, 1 mg/ml, 2 mg/ml), PEGDA molecular weight (500, 740 and 3400 Da), and PEGDA concentration (10%, 20%, and 30% w/w) as well as irradiation parameter, laser power (0.5 μW, 1 μW, 2μW, 4μW, 8μW) were optimized in terms of dynamic range ($F_{max}/F_{min}$), sensor length and response time. The images of microtips were taken with a CMOS camera (MU1000, AmScope) on an inverted light microscope (Olympus, CKX41). Images were analyzed for tip length using the image processing software, ImageJ. Sensor response time within the linear sensing range was calculated as 95% of the time taken to respond to a change in analyte concentration. The morphology of microtip sensors was examined by cryo-scanning electron microscopy (cryo-SEM, Nova NanoSEM, FEI). Flash freezing of microtips was achieved using liquid nitrogen slush. After sputter coating with platinum, imaging was performed under vacuum.

For the rest of the characterization experiments, precursor solution of 1 mg/ml final GCaMP3 concentration, 10% $PEG_{740}DA$ and 1% IR2959 in MOPS buffer was cured for 10 sec with the laser power of 1 μW to fabricate the sensors. To examine the sensor stability, change in the dynamic range of the sensor was monitored for four weeks. The stability measurements were performed by switching the sensor from zero-calcium to calcium-saturation buffer and leaving the sensor in zero-calcium buffer between measurements. The effect of PEGDA molecular weight ($PEG_{740}DA$ and $PEG_{3400}DA$) on the protein-release rate was determined over the course of six hours by taking hourly measurements of the fluorescence emission intensity in high calcium buffer (39 μM, free calcium). Sensor stability was reported as a change in dynamic

range. The excitation light intensity (12.5 nW, 25 nW, 50 nW and 75 nW) was modulated to investigate the photobleaching effect of excitation light source on the sensor. During these measurements, sensors were continuously exposed to the light for three hours. The ratio of $F/F_0$ was used to express the fluorescence intensity change relative to its starting signal. F is the fluorescence emission intensity at any time and $F_0$ is the fluorescence emission intensity at time zero.

Sensor selectivity was tested for two common physiological relevant divalent cations, zinc (Zn(II)) and magnesium (Mg(II)). The ratio of $F/F_{min}$ was used to evaluate the sensor response to free zinc, magnesium and calcium ions at the highest concentration levels. Following equation was used to calculate the free zinc concentration; $[Zn^{2+}]=K_d[ZnEGTA]/[EGTA]$. $K_d$ of EGTA for zinc at pH 7 was taken as 7.09 nM and increased by 0.02 log unit per 0.01 increase in pH [20]. Free $[Mg^{2+}]$ level was calculated using Maxchelator.

Sensor microtip calibration was carried out via sequential insertion into buffers with known $[Ca^{+2}]_{free}$ made using stock solutions of CaEGTA and $K_2$EGTA at pH 7.4. $(F-F_{min})/F_{min}$ was plotted against $[Ca^{+2}]_{free}$ concentrations and was fit to Hill equation to determine $K_d$ and sensitivity of the sensor. $K_d$ (dissociation constant) was calculated by according to the Hill equation, $Y = X^n/(K_d^n + X^n)$. All measurements were conducted in triplicate and data points were collected every 100 ms averaging fluorescence emission intensity between 512 and 515 nm. The limit of detection (LOD) was determined using the Hill equation at 3.3 times of the standard deviation of background[21].

2.6. Statistical analysis

All experiments were performed in triplicate. All statistical analyses were implemented using statistical analysis software (Origin Pro). Analysis of variance (ANOVA) with Tukey's post-hoc test was used for statistical evaluation of experimental data ($p < 0.05$).

## 3. RESULTS AND DISCUSSION

### 3.1. Evaluation of irradiation parameters and precursor solution components

*3.1.1. GCaMP3 activity can be retained by carefully monitoring photopolymerization parameters*

Ligand induced conformational change in the protein is crucial for sensor function. The conditions of photopolymerization create a new local physical and chemical environment around the GCaMP3 protein, which can alter both protein-ligand binding affinity and ligand induced structural changes[4]. Therefore, we first investigated the effect of the photopolymerization parameters on GCaMP3's fluorescent response to $Ca^{+2}$. Protein activity with respect to its dynamic range was defined as the ratio of calcium-saturated GCaMP3 fluorescence emission intensity to calcium-free emission intensity ($F_{max}/F_{min}$). Each parameter of in situ photopolymerization, including UV light exposure, presence of photo-initiator and polyethylene glycol diacrylate (PEGDA) was evaluated individually and in combination by using $F_{max}/F_{min}$.

High intensity or deep UV exposure (wavelength < 365 nm) can cause protein denaturation[22], and therefore prolonged exposure of UV during photopolymerization might cause detrimental outcomes to GCaMP3 function. In this case protein activity dropped significantly when GCaMP3 was exposed to UV light alone (no photo-initiator) at all tested UV exposure times but this activity loss was not further intensified over time (Fig. 2a). Next we examined the impact of UV exposure in the presence of photoinitator (PI), Irgacure 2959 (IR 2959). IR2959 is the most

commonly used commercially available photoinitator for photoencapsulation of cells, proteins and other biomolecules into hydrogel scaffolds owing to its well-proved efficiency and cytocompatibility[22,23]. Highly reactive free radicals, however, are released during photopolymerization as a result of the UV-induced decomposition of the photoiniator. These free radicals can attack aromatic, sulfur-containing amino acid side chains and C-H sites on proteins and thereby, lead to protein oxidation and degradation[24]. In the case of GCaMP3, protein activity remained constant upon addition of photoinitiator before light exposure, but decreased progressively in the presence of PI and prolonged UV exposure (more than 10 seconds) leading to significant loss in protein activity (Fig. 2a). Furthermore, UV induced activity loss was more pronounced in the presence of photoinitiator compared to UV light alone suggesting possible protein denaturation due to light-induced generation of free radicals by photoinitiator.

a.

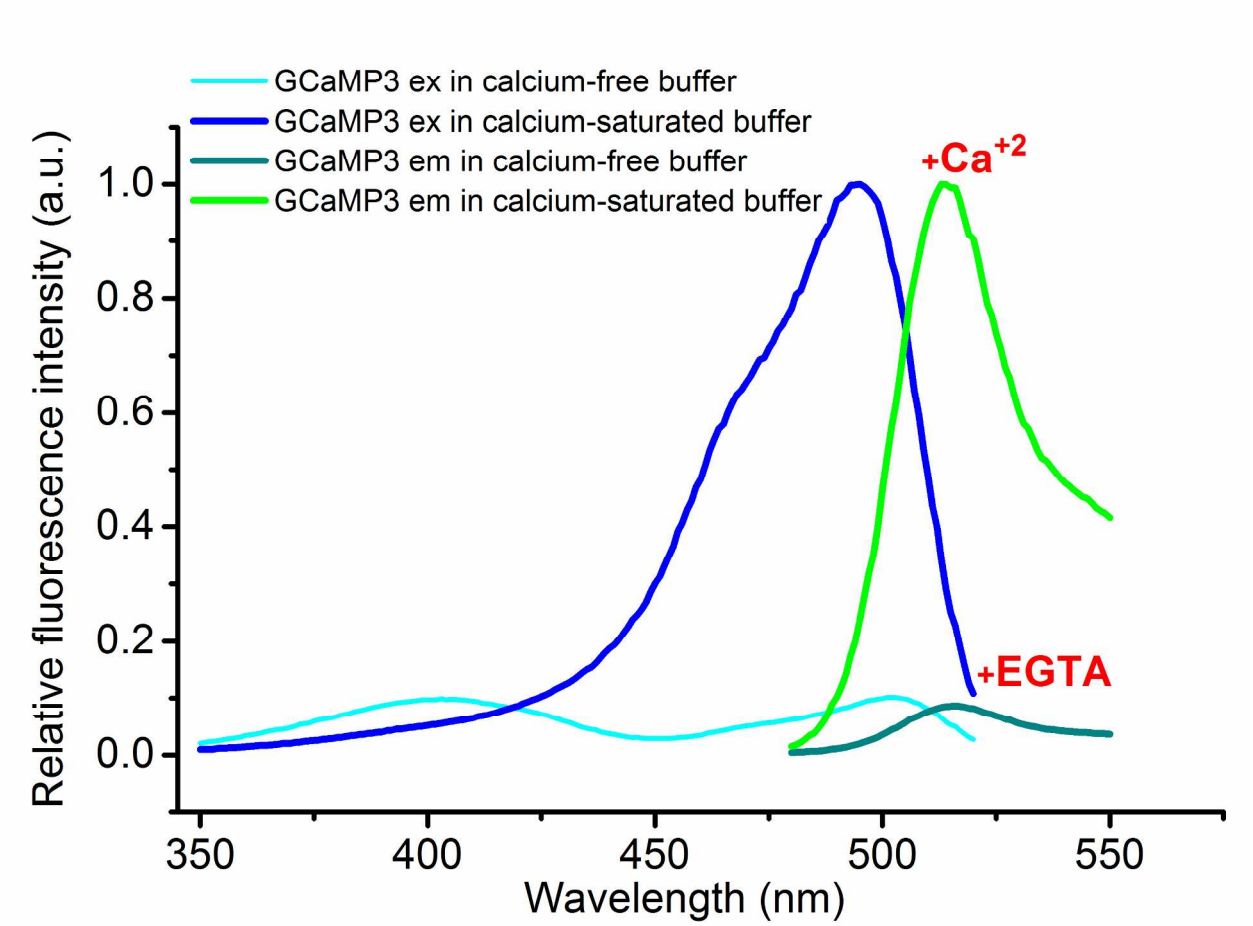
GCaMP3 ex in calcium-free buffer
GCaMP3 ex in calcium-saturated buffer
GCaMP3 em in calcium-free buffer
GCaMP3 em in calcium-saturated buffer
+Ca+2
+EGTA
Relative fluorescence intensity (a.u.)
1.0
0.8
0.6
0.4
0.2
0.0
350
400
450
500
550
Wavelength (nm)

b.

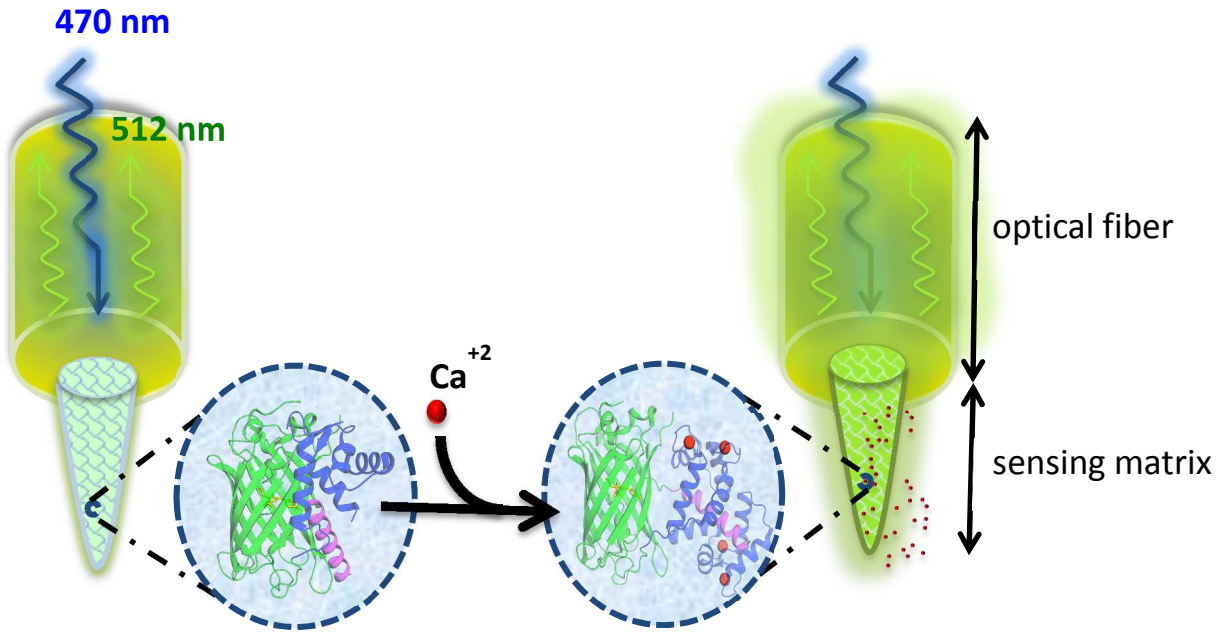
470 nm
512 nm
Ca+2
optical fiber
sensing matrix

**Figure 1. GCaMP3 and sensor characteristics. a.** Fluorescence spectra of GCaMP3 in the absence and presence (39 μM) of calcium in MOPS buffer. The fluorescence intensity of each measurement was normalized to the peak of calcium saturated spectrum. The cyan and blue colored lines indicate GCaMP3 excitation spectrum in calcium-free buffer and in calcium-saturated buffer while dark cyan and green colored lines show GCaMP3 emission spectrum in calcium-free buffer and in calcium-saturated buffer, respectively. **b.** Schematic representation of GCaMP3 optrode. Hydrogel protein sensor was grown at the end of a multimode optical fiber. GCaMP3 consists of a cpEGFP (green) flanked between calcium binding protein calmodulin (blue) and calmodulin binding peptide M13 (magenta). PDB:3SG3. GCaMP3 sensor was excited with 470 nm LED light (represented by the blue arrow) and emitted light was collected at 512 nm (represented by the green arrows) as the sensor response. Upon calcium binding, interaction of calmodulin with M13 induces conformational changes in the fluorophore environment causing an increase in fluorescence emission.

We hypothesized that PEGDA might offer some protection to the protein during photopolymerization. To explore the effect of PEGDA on free radical mediated protein denaturation, PEGDA (740 Da) was added to the precursor solution (10% w/w) and exposed to UV light for varying durations. The introduction of PEGDA preserved the protein activity and even increased the activity slightly above that of control sample (protein before light exposure) at all exposure times. Previous studies have shown an increase in fluorescence emission signal from the enhancement in quantum yield in the presence of PEG[25]. Further, adding PEGDA into photoinitiator-protein precursor solution likely decreased the effect of free-radical mediated activity loss, and this loss only became significant at UV exposure of 60 seconds. Protein

activity retention at lower exposure times could be attributed to stealth and shielding properties coming from PEG backbone of PEGDA, which might restrict the interaction between free radicals and protein by increasing solution viscosity[22]. Additionally, free radicals generated by photoinitiator tend to attack and propagate through multiple carbon-carbon double bonds of monomer (acrylate functional groups of PEGDA) [26]. Thus, the presence of acrylate groups on monomer might also provide some protection for the protein by acting as a free radical scavenger[27].

Regardless of activity loss at long exposure times, good GCaMP3 activity could be maintained in a PEGDA matrix by minimizing the irradiation time even under high UV energy exposure (2 W/cm$^2$). These initial results were used to set the UV exposure time for the remaining studies.

a. b.

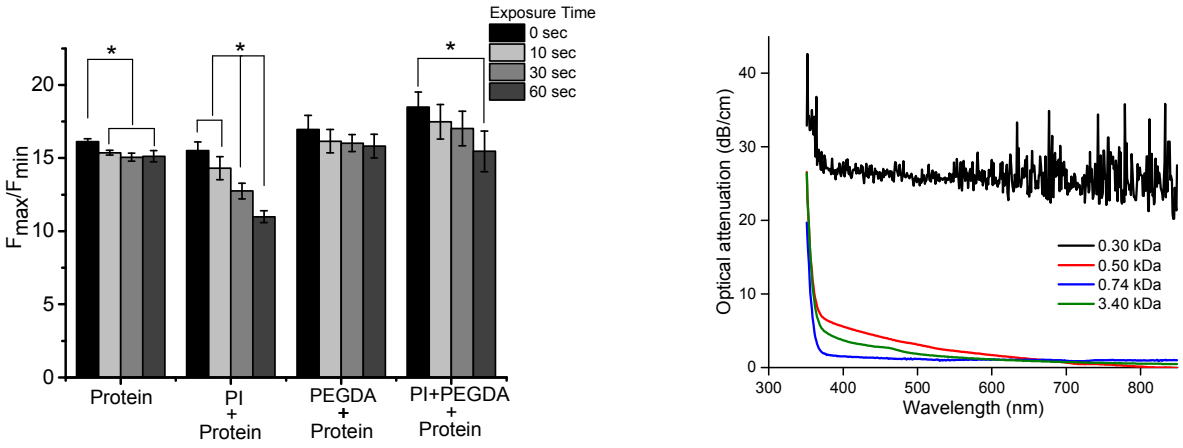


**Figure 2. Effect of photopolymerization parameters (UV light exposure, presence of photoinitiator, PI and PEGDA) on GCaMP3 activity (a) and optical attenuation of the resulting matrix (b). a.** Exposure to UV light (325 nm, power density of 2 W/cm$^2$ at the end of 1000 μm core multimode fiber) caused significant reduction in GCaMP3 activity as measured by

the ratio of the maximum and minimum fluorescence response to high and low calcium concentrations. The addition of photoinitiator (1% w/w) resulted in a more pronounced activity loss at longer UV exposure times (>10 seconds). The introduction of $PEG_{740}DA$ (10% w/w) showed no change in protein activity. Similarly, the combination of PEGDA with photoinitiator did not produce a significant loss in protein activity except for 60 seconds of UV exposure suggesting that PEGDA provides some protection for protein. One asterisk (*) indicates 0.05 significance level. **b.** Spectral attenuation for PEG hydrogels with different PEGDA molecular weights. PEGDA molecular weight can be used to tune the optical attenuation of precursor solution.

*3.1.2. Optical transparency of precursor solution depends on the PEGDA molecular weight.*

Optical transparency of the precursor solution is crucial for spatial resolution of the microtip as well as proper excitation of the protein and collection of the emitted fluorescence signal at the end of optical fiber. To optimize the precursor compositions, we measured the attenuation spectra of hydrogels with different molecular weights of PEGDA. Low molecular weight PEGDA (0.3 kDa) created white opaque strongly scattering precursor solutions (Supporting information Fig. S4a) and thereby, led to the greatest optical loss (≈30 dB $cm^{-1}$) in the visible range (400-700 nm) (Fig. 2b). The optical transparency of the precursor solutions noticeably increased with PEG molecular weight over 300 Da and precursor solution made from the higher molecular weights PEG monomers ($PEG_{500}DA$, $PEG_{740}DA$, and $PEG_{3400}DA$) showed better optical transparency and so, lower attenuation in the visible range compared to $PEG_{300}DA$. The solubility of PEG comes from hydrogen bond formation between the electron-rich ether oxygen of PEG and water molecules[28]. As the linear chain length of PEG increases and so does the

chance of hydrogen bonding formation between water molecules and oxygen atoms in the monomer chain.

### 3.2. Effect of Photopolymerization Conditions on Microtip Optrode Geometry and Sensor Performance

*3.2.1. The uniform refractive index fluctuation and thereby, microtip growth depends primarily on the optical transparency of the precursor solution*

Sensor microtip geometry is primarily defined by the self-focusing of the light beam as a result of the refractive index change during photopolymerization[29]. As the monomer crosslinking proceeds upon light exposure, pore formation leads to refractive index modulation at the solid/liquid interface and reduces the transparency of the solution leading to microtip formation through self-focusing effect[23]. Among the precursor solutions tested, successful hydrogel microtip formation was observed with the ones made from the higher molecular weights PEG monomers ($PEG_{500}DA$, $PEG_{740}DA$, and $PEG_{3400}DA$) at the end of the optical fiber. However, precursor solution made from low molecular weight, $PEG_{300}DA$ did not produce any hydrogel microstructure at the end of the fiber by blocking the UV light (UV power set to 5 μW at the end of 50 μm core multimode optical fiber) propagation (data not shown). Taking all these into consideration, microtip characterization experiments were performed using $PEG_{500}DA$, $PEG_{740}DA$, and $PEG_{3400}DA$ in order to create reproducible microtip structures.

*3.2.2. Optrode microtip geometry and sensitivity can be controlled by adjusting UV light intensity.*

The microtip geometry (sharpness and length) of the sensor material at the end of the optical fiber can be altered by controlling the energy of incident radiation, which depends on the UV laser power and exposure time. Based on results summarized in Fig. 2a, irradiation time was fixed at 10 seconds by setting the laser power density below 2 W/cm$^2$ (at the end of 50-μm core multimode optical fiber) to minimize any detrimental effect coming from high UV energy exposure on protein activity. Irradiation power was varied for 10 seconds from 0.5 to 8 μW corresponding to power densities of 0.1 and 0.8 W/cm$^2$, respectively. Hydrogel polymerization did not occur reliably on the optical fiber after 10 seconds when irradiation power was below 0.5 μW suggesting that the total incident energy applied was lower than threshold energy of polymerization under those given conditions. Threshold incident energy of polymerization is the minimum energy required to initiate the photochemical reaction and thereby photopolymerization [30]. To obtain a reasonable microtip length after 10 seconds of light exposure, the total irradiation power was varied from 0.5 μW to 8 μW at the end of 50 μm diameter core multimode optical fiber using a combination of neutral density filters. The microtips became progressively longer and more distorted in shape upon exposure to higher laser powers (Fig. 3a-e). Microtip shape distortion would be ascribed to poor structural integrity of the hydrogel matrix that can easily bend or collapse at geometries of high aspect ratios. Even though tips grown at 0.5 μW showed the best response times when switching from zero-calcium to calcium-saturation and from calcium-saturation to zero-calcium buffers (Supporting information Table S1), maximum sensor calcium response was observed with microtips fabricated using UV laser power at 1.0 μW. Lower calcium response of sensors made at 0.5 μW is the result of small sensor sizes leading to inadequate sensor protein concentration, which in turn resulted in insufficient signal to noise during testing. Sensors fabricated at the power levels above 2 μW

resulted in distorted tip shapes, long response times and low calcium response probably due to large bulky sensor sizes and the resulting poor diffusion rates. Therefore, optrode microtips were grown at 1 μW for the remainder of the characterization experiments.

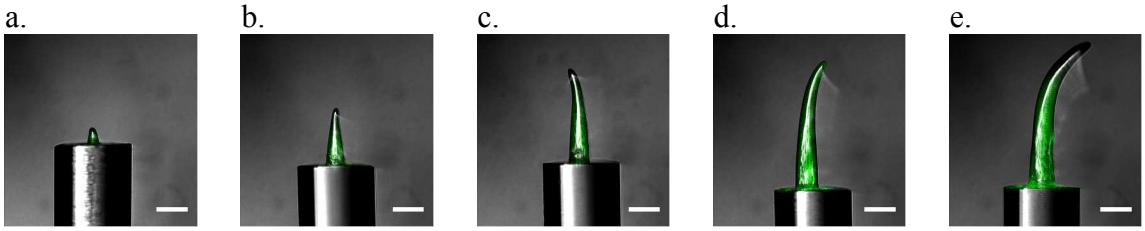


**Figure 3.** The hydrogel microtip became longer but more distorted in shape with increase in UV light intensity used for sensor fabrication. The overlay of fluorescence and bright field images of microtips grown from the precursor solution composed of 10% w/w $PEG_{740}DA$, 1% w/w IR2959 and 0.25 mM GCaMP3 protein concentration using UV laser power at a. 0.5 μW b. 1 μW c. 2 μW d. 4μW e. 8 μW (scale bars:100 μm) for 10 seconds.

*3.2.3. Protein concentration within the hydrogel matrix can affect sensor sensitivity significantly below a minimum concentration.*

The resolution and sensitivity of any sensor depends on the signal to noise (S/N) ratio. Being nearly isotropic, fluorescence is emitted in all directions, causing only 1% or less of the total fluorescence emission signals to be collected with typical sensor geometries and photodetectors[31]. Thus, the optimization of a biorecognition element concentration is crucial for defining sensor sensitivity. The normalized maximum calcium response, $F_{max}/F_{min}$, of the sensors grown using different GCaMP3 concentrations (0.25, 0.5 and 1.0 mM) was measured to determine an optimum protein concentration within sensor hydrogel matrix (Supporting information Fig. S4b). The normalized maximum calcium response of the sensor did not show a significant increase when the final protein concentration was at or above 0.5 mM in hydrogel

matrix. Sensor microtips were therefore grown at a final protein concentration of 0.50 mM for the remaining studies to collect reasonable fluorescent signal as well as to minimize the amount of protein used in the sensor hydrogel matrix.

*3.2.4. Structural properties of the sensor matrix and in turn sensor performance are governed by monomer molecular weight and concentration in the precursor solution.*

The geometry and microstructure of the sensor matrix will have a direct effect on the sensor performance and should ideally be tunable for different applications. A sensor hydrogel matrix should have structural properties that ensure the transport of the ligand and allow for ligand-induced conformational changes of the protein for signal transduction while minimizing sensor protein release (i.e. leaching) from the matrix. The ability to tune hydrogel properties by varying monomer molecular weight and concentration in the precursor solution can be used to obtain a network fulfilling aforementioned requirements[12,32]. We optimized microtip geometry and the matrix microstructure by systematically varying the molecular weight and concentration of PEGDA monomer in the hydrogel precursor solution.

We first fabricated hydrogel discs to understand the effect of different precursor compositions on network properties, namely crosslinking density, mesh size and swelling ratio using equilibrium swelling theory[19,33] (Fig. 4a and 4e). Significantly high swelling ratios with low crosslinking densities were obtained when molecular weight of PEGDA was increased from 500 to 3400 Da at the same monomer concentration, 10% w/w, in the precursor solution (Fig. 4a). Loosely crosslinked hydrogel network of $PEG_{3400}$Da also resulted in significantly large mesh sizes. On the other hand, more densely packed networks were created with higher crosslinking

densities when monomer concentration was increased from 10 to 30% w/w in precursor solution of $PEG_{740}DA$ (Fig. 4e).

Along with bulk the hydrogel properties deduced from the equilibrium swelling theory, we used cryogenic-temperature scanning electron microscopy (cryo-SEM) to obtain more direct knowledge regarding the fully hydrated microtip surface morphology. Increasing the PEGDA monomer molecular weight resulted in larger surface pores with more honeycomb-like microstructure but had no significant impact on the microtip size at given PEGDA concentration of 10% w/w (Fig. 4b-d; Supporting information Fig. S5-S7a). On the other hand, increasing the PEGDA monomer concentration in precursor solution of $PEG_{740}DA$ created highly crosslinked hydrogel network with progressively longer microtips because of the increase in crosslinking density (Fig. 4f-h; Supporting information Fig. S6-S7b). Such a significant change in microtip size can also be explained by an increase in available acrylate groups, which causes more layers to be built on top as UV light propagates through the precursor solution. Overall, structural properties of bulk hydrogel showed good correlation with microtip surface morphology.

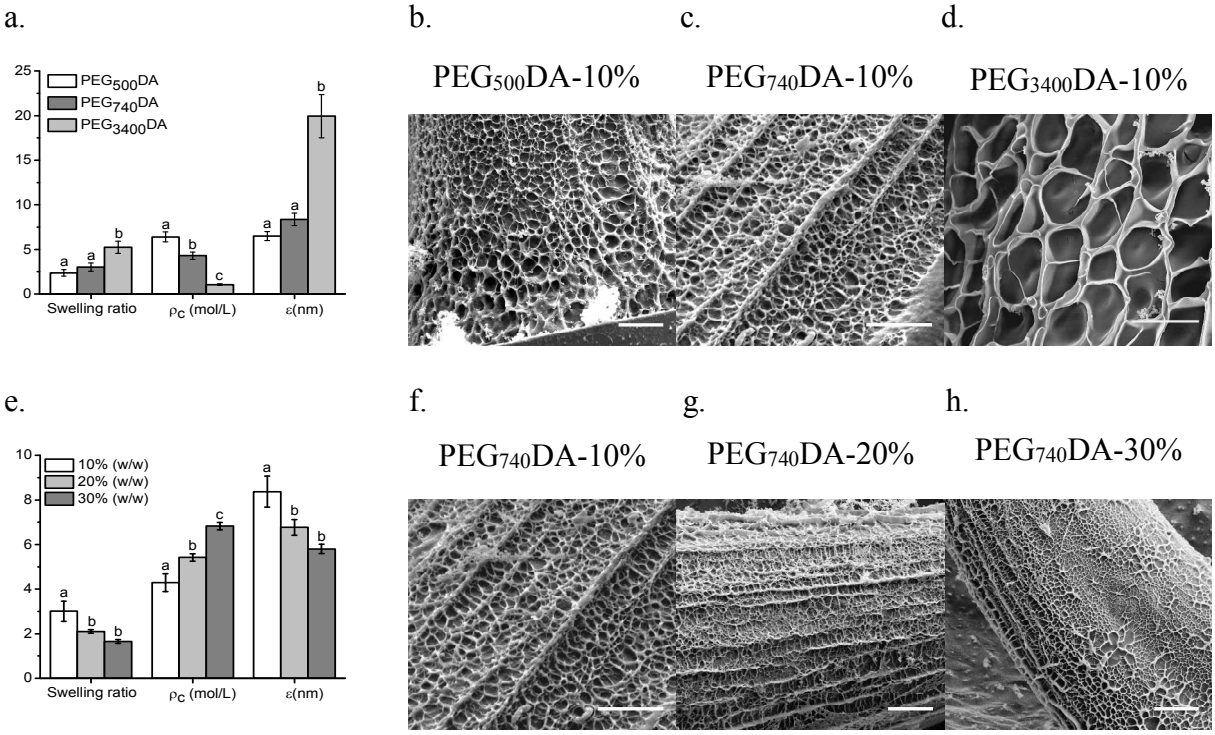


**Figure 4. Structural properties of hydrogel matrix and microtip morphology are affected significantly by PEGDA molecular weight and concentration in the precursor solution. a.** Larger swelling ratios and mesh sizes (ε) with corresponding low crosslinking densities (ρc) were obtained when molecular weight of PEGDA was increased from 500 to 3400 Da. The representative cryo-SEM images of hydrogel microtips fabricated from 10% (w/w) of **b.** $PEG_{500}DA$, **c.** $PEG_{740}DA$, **d.** $PEG_{3400}DA$ showed similar trend with estimated structural properties of bulk hydrogel samples (scale bars: 5 μm). **e.** Highly crosslinked ($\rho_c$) hydrogel matrix with smaller swelling ratios and mesh sizes (ε) were obtained when the concentration of PEG740DA in the precursor solution increased from 10 to 30% (w/w). Similar trend was observed with the representative cryo-SEM images of microtips made with PEG740DA concentration of **f.** 10%, **g.** 20% and **h.** 30% (w/w) in the precursor solution respectively (scale bars: 5 μm). Treatments (n=3) with no letters in common are significantly different ($p< 0.05$).

As shown above, the sensor's hydrogel network impacts the photopolymerization and resulting microtip structure during sensor production. In addition, the resulting pore structure should impact diffusion of analyte to the sensor protein and the retention of the sensor protein during use. Thus, the final sensor response time and stability will also be directly affected by the PEGDA molecular weight and concentration. In both cases, the hydrogel mesh size relative to the size of analyte/protein is the major factor affecting the diffusion rates[34].

We next characterized the microtip sensors of various PEGDA molecular weights (500, 740 and 3400 Da) at the same concentration (10%w/w) to determine how different precursor composition and thereby, hydrogel network properties affect protein sensor performance. Sensor performance was evaluated in terms of calcium response times (Fig. 5a) and normalized maximum calcium response (Fig. 5b). Significantly long calcium response times were observed with hydrogel microtips fabricated from $PEG_{500}DA$ while sensors grown with $PEG_{3400}DA$ showed the best response times (Fig. 5a). As examined before in Fig 4a., increasing PEG molecular weight led to lower crosslinking density and larger mesh sizes that might facilitate rapid diffusion of analyte into hydrogel network and result in better response time. However, sensors grown with $PEG_{3400}DA$ were mechanically unstable and easily detachable from fiber core during rinsing steps leading to the lowest sensor dynamic range. A clear tradeoff between diffusion rates and structural integrity was observed at longer chain lengths. This general tendency would be an effect of poor crosslinking density with insufficient structural integrity at longer monomer chain length. In contrast, there was no apparent trend for normalized maximum calcium response of sensors grown with different PEG molecular weights (Fig. 5b). In this case, significantly low normalized calcium response was obtained with sensors made with $PEG_{3400}DA$. Such variation in sensor calcium response can be explained with highly porous microstructure of

sensors fabricated from $PEG_{3400}DA$ (Fig 4d), which might bring in the possibility of sensor protein leachout and thereby, decrease signal to noise ratio.

To address this concern, fluorescence emission signal of GCaMP3 from microtip sensors made with PEGDA molecular weights of 740 Da and 3400 Da was examined. These studies were designed to measure protein leaching and measurements taken hourly for 1 minute in high calcium buffer to minimize photobleaching. As presented in Fig. 5c, fluorescence emission signal dropped drastically (30% loss in the signal) after the first hour of monitoring in the case of the sensors fabricated with $PEG_{3400}DA$. This sharp drop in fluorescence emission was a clear indication of sensor protein leachout from microtip hydrogel matrix of $PEG_{3400}DA$ because of observed large mesh sizes (Fig. 4a) and surface macropores (Fig. 4d). However, fluorescence signal reduction of microtip sensors made with $PEG_{740}DA$ remained around 10% even after 6 hours of monitoring. $PEG_{740}DA$ gave the best sensor performance among the monomers tested. Sensor microstructure or mesh size might be the primary parameter defining sensor sensitivity because of the inverse relationship between network density and mesh size. Densely packed hydrogel network might restrict ligand-induced conformation change and in turn lower sensor dynamic range. Mesh size of hydrogels fabricated with $PEG_{740}DA$ (Fig. 4a) might be small enough to restrict diffusion of GCaMP3 greatly while providing a confined space that enables a favorable protein conformational change. Thus, all optimization experiments were performed with sensors fabricated using $PEG_{740}DA$ in the following studies.

We also examined the performance of microtips grown with varying concentrations of $PEG_{740}DA$ (10%, 20% and 30% w/w). Sensor dynamic range decreased significantly at higher hydrogel matrix monomer concentrations (Fig. 5d) when $PEG_{740}DA$ concentration was increased from 10 to 30% (w/w) in the precursor solution exhibiting again the strong correlation between

sensor performance and mesh size. In addition, microtip sizes and in turn sensor response times dramatically increased with concentration (Supporting information Fig. S7b-c). Observed trend in sensor performance with increasing $PEG_{740}DA$ concentration can be explained by higher crosslinking densities (Fig. 4e) and smaller surface pores (Fig.4f-h) of microtips that might restrict sensor protein movement required for signal transduction as well as calcium diffusion within the hydrogel matrix. Therefore, the remaining optrode performance characterization experiments were conducted using hydrogel micro-optrodes fabricated from a fixed $PEG_{740}DA$ concentration of 10% (w/w). Overall, strong correlation between sensor performance and hydrogel structural properties was observed.

a.

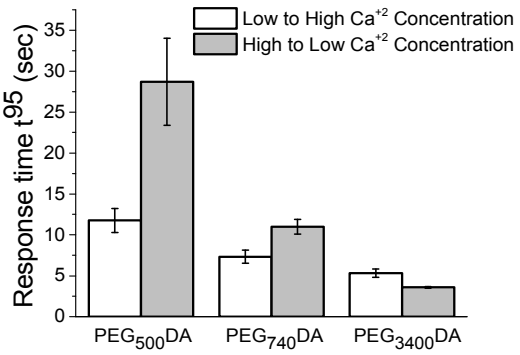


b.

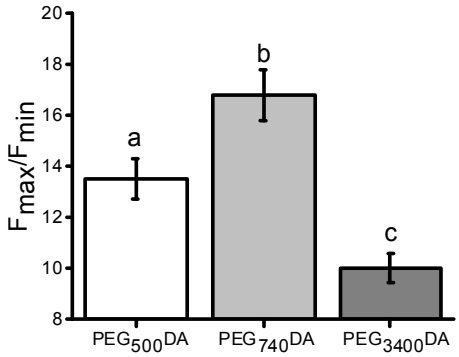


c.

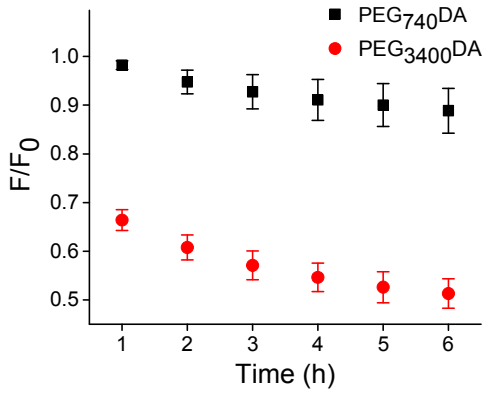


d.

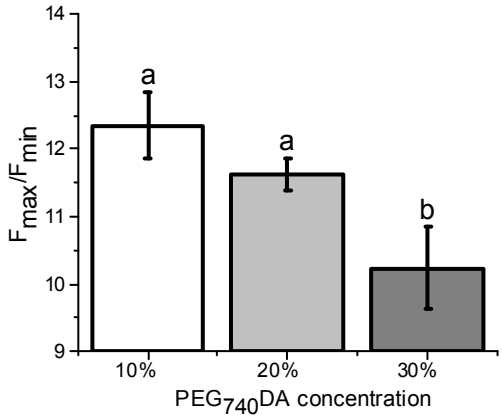

**Figure 5. Micro-optrode sensors grown with intermediate PEGDA molecular weight result in the best combination of dynamic range, response time, and stability. a.** Sensor response times decreased drastically with increasing PEGDA molecular weight in precursor solution when switching from zero-calcium to calcium-saturation and from calcium-saturation to zero-calcium buffers. **b.** Sensor calcium response significantly affected by PEGDA molecular weight used in precursor solution and the best calcium response was observed with micro-optrodes grown with $PEG_{740}DA$. $F_{max}$: calcium-saturated GCaMP3 fluorescence emission intensity, $F_{min}$: calcium-free GCaMP3 fluorescence emission intensity. **c.** Protein release from microtip sensors was monitored as fluorescence signal reduction over time and the highest release was obtained with microtips fabricated from $PEG_{3400}DA$ at all time points. F: GCaMP3 fluorescence emission intensity at a given time, $F_0$: GCaMP3 fluorescence emission intensity at time zero. **d.** Sensor calcium response revealed a significant decreasing trend with $PEG_{740}DA$ concentration when monomer concentration was increased from 10 to 30% (w/w) in the precursor solution. Treatments (n=3) with no letters in common are significantly different ($p< 0.05$).

3.3. Sensor stability

Protein-hydrogel sensors should show functionally stable characteristics over a period of time (from weeks to months) for practical sensor applications. The long-term stability of hydrogel-based sensors mainly depends on the hydrogel structural integrity and biomolecule stability. To investigate this issue, sensors fabricated with $PEG_{740}DA$ were stored at room temperature in the buffer for four weeks and sensor dynamic range change ($F_{max}/F_{min}$) was monitored during this period. Microtip sensor signal showed an insignificant decrease in the first two weeks compared to the initial value and stabilized after the third week (Fig. 6a). This decrease would be

attributed to degradation of PEGDA in the buffer[35] and so substantial increase in protein release from the microtip as well as protein degradation over time.

a. b.

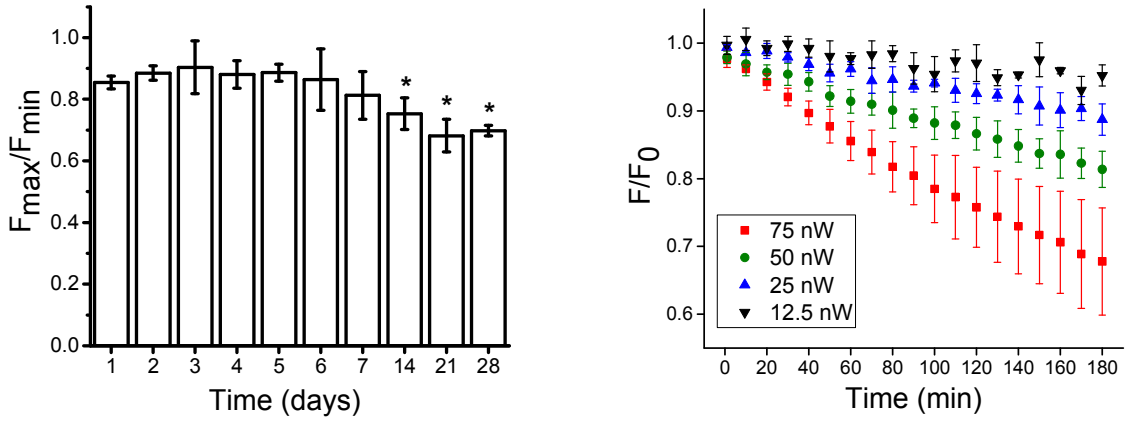


**Figure 6. Microtip sensor stability over time (a) and varying excitation light powers (b)** . **a.** Sensor normalized calcium response decreased gradually in the buffer over 4 weeks. One asterisk (*) indicates statistically significant difference between the mean of $F_{max}/ F_{min}$ at the given time compared to the mean at time zero ($p<0.05$). $F_{max}$: calcium-saturated GCaMP3 fluorescence emission intensity, $F_{min}$: calcium-free GCaMP3 fluorescence emission intensity. **b.** Photobleaching of fluorescence emission signal of GCaMP3 was severe when microtip sensor was excited at high LED (470 nm) power levels (>25 nW), but almost no photobleaching was observed when excited with LED power intensity of 12.5 nW over 3 hours continuously. F: GCaMP3 fluorescence emission intensity at a given time, $F_0$: GCaMP3 fluorescence emission intensity at time zero.

3.4. Photobleaching of protein optrode

Photobleaching of fluorescent protein and in turn lower emission signal can reduce the maximum attainable sensitivity (S/N) of the sensor. Photobleaching can be defined simply as irreversible fluorescence loss upon excitation light exposure. This loss takes place when fluorophore molecule in the excited singlet or triplicate state undergoes detrimental photochemical reaction with a reaction rate that is a function of the excitation light intensity[36]. In this regard, we monitored the change of sensor fluorescence emission intensity over 3 hours upon continuous exposure to varying excitation light intensities (Fig. 6b). Fluorescence signal of sensors compared to that of time zero dropped significantly after 20, 30, 60 and 140 minutes continuous exposure to the excitation LED power of 75 nW, 50 nW, 25 nW and 12.5 nW, respectively ($p<0.05$). Overall increasing the excitation light power caused a reduction in the fluorescence emission but this reduction was less severe at the low power levels of 12.5 nW and 25 nW (below 10% fluorescence emission loss after 3 hours). Therefore, we performed all calibration and sensitivity experiments with the excitation LED power of 12.5 nW to minimize the photobleaching effect during the measurements.

### 3.5. Sensitivity and selectivity of the micro-optrode sensor

Based on the above studies, $PEG_{740}DA$ was selected and used at a concentration of 10% w/w in the precursor solution for the final calcium sensor design. Hydrogel sensors were fabricated using UV laser power at 1 μW for 10 seconds (as discussed in Section 3.1.1 and 3.2.1). We then characterized the sensor's performance and measured the effective binding affinity, limit of detection, dynamic range, sensitivity, reversibility, and selectivity for calcium relative to other divalent cations.

To determine the effective binding affinity ($K_d$) for calcium, the sensor response to varying free calcium concentrations in MOPS buffer was measured and compared to the response of free protein in buffer (Fig. 7a). Using a Hill equation model, an effective $K_d$ of GCaMP3 in buffer was found to be 194±4.46 nM with Hill coefficient of 2.6, consistent with previous reports for GCaMP3[37]. Surprisingly, the calcium-binding affinity of GCaMP3 when incorporated into microtip optrode increased to an effective $K_d$ of 122±4.81 nM with Hill coefficient of 1.4 ($R^2$=0.998) (Fig. 7a). PEG could be responsible for this effect through a couple of possible mechanisms. First, the increased binding affinity could be attributed to fluorescence quantum yield enhancement in the presence of PEG[25] enhancing the measured response. Alternatively, PEG might stabilize a conformational state of the protein and increase the affinity or accessibility of calcium binding sites.

The limit of detection (LOD) was calculated using 3.3 times the standard deviation of the intensity of the background signal and the standard deviation of background signal was measured to be 0.111 (n = 48). After fitting the standard deviation of background signal into Hill equation, the LOD of sensor for free calcium was calculated to be 4.3 nM. The calcium titration curve indicated a good linear relationship between the logaritmic values of fluorescence intensity ratio of $(F-F_{min})/(F_{max}-F)$ and of free calcium concentration in a range of 39 nM to 1 μM ($R^2$=0.99) (Fig 7b). The linear range of GCaMP3 remained unchanged for the sensor relative to the protein in solution. We also investigated the reversibility of the sensor by repeatedly exposing the optrode to 0 and 39 μM free calcium in 30 mM MOPS, 100 mM KCl;KOH at pH 7.4. As shown in Fig. 7c, the sensor was highly reversible and returned to roughly the same fluorescence emission signal, even after 3 cycles of low to high calcium buffer exposure.

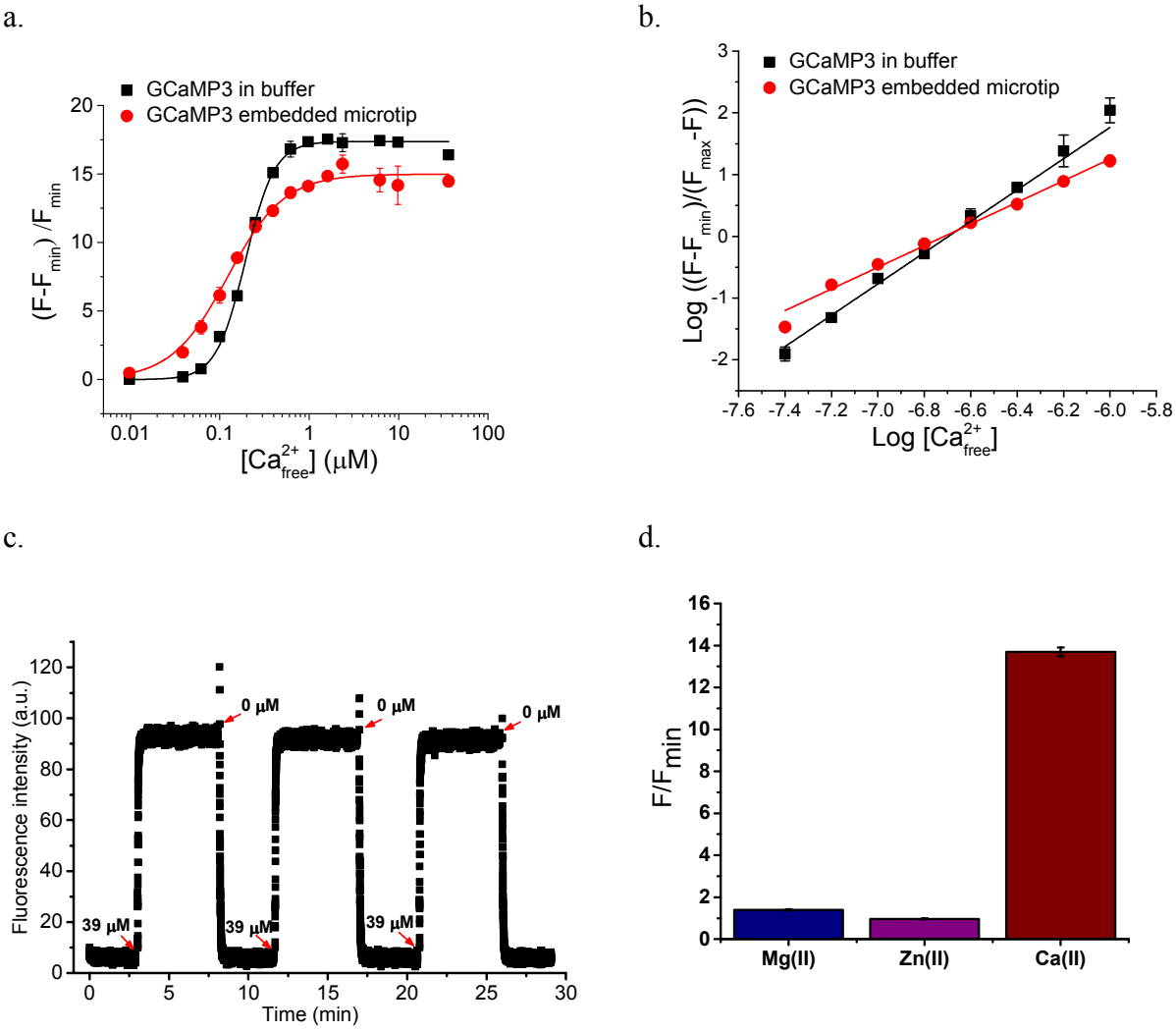


**Figure 7. Microtip sensor calibration, reversibility and selectivity**. **a.** Calcium titration curve of GCaMP3 in buffer and when embedded into hydrogel microtip. Calcium binding affinity of GCaMP3 in buffer was calculated to be 194 nM while $K_d$ of sensor was found to be 122 nM. Solid curves represent fits to the Hill equation. LOD of the sensor was calculated to be 4.3 nM **b.** Logarithmic titration curves of protein and sensor showed a similar linear range from 39 nM to 1 uM **c.** Microtip sensor signal was highly reversible. Arrows show the time points at which the calcium-free buffer was switched to the corresponding concentration on the figure. **d.** GCaMP protein optrode was highly selective to calcium over other divalent cations at physiologically

relevant free ion concentrations. Mg (II): 5 mM; Zn(II): 5 nM; Ca(II): 39 μM. F: fluorescence emission at given ion concentration; $F_{min}$: fluorescence emission in ion free buffer.

The selectivity of sensor was evaluated by comparing the calcium response to other divalent cations (magnesium and zinc) (Fig. 7d). Sensor fluorescence emission response was measured when exposed to physiologically relevant free ion concentrations of magnesium (Mg(II)) and zinc (Zn(II)); 5 mM[38] and 5nM[39], respectively. Calmodulin (CaM) is the calcium-binding domain of GCaMP3. CaM has two globular domains (C- and N-domains), and there are two helix-loop-helix calcium-binding motifs (EF-hand motifs) within each domain[40]. CaM reorients its four-helix bundles upon binding calcium. Mg(II), as being the closest divalent homologue of calcium, caused a slight increase in sensor fluorescence emission response at the highest physiologically relevant concentration tested (5mM) (Fig. 7d). Even though Mg(II) binding to calmodulin is not expected to induce any conformational changes that is characteristic of calcium binding, N-domain of CaM has low binding affinity for Mg(II) in the absence of calcium[41] which might explain small increase of sensor response. Zinc produced no detectable change in fluorescence emission response. As previously reported[40] when Zn (II) binds to CaM, it does not induce any global conformational change and so causes no change in GCaMP fluorescence emission. In conclusion, GCaMP optrode retained its high selectivity for calcium over other divalent cations such as Mg (II) and Zn (II) in the PEG acrylate hydrogel environment of the optrode sensor.

**4. Conclusions**

Optically transparent, spatially definable, and biocompatible hydrogels are in demand for biophotonic applications including biosensing. While various materials are available, few show both optical transparency and compatibility with biomolecules such as proteins. In addition, the

recent engineering of novel genetically encoded molecular sensors, which have mostly been implemented in imaging applications, also dramatically increases the number and range of proteins as biosensor recognition molecules. We therefore explored a PEG-diacrylate hydrogel system as a sensor matrix for a GCaMP3, as a model genetically encoded molecular sensor. The diacrylate monomers provide spatial patterning of sensor geometry via light induced photopolymerization and good optical transparency. The PEG moieties in PEGDA offer a hospitable environment for the protein and opportunity to tune the matrix microstructure and pore size.

In this sense, we investigated the role of precursor solution composition and irradiation parameters on the protein bioactivity during photoencapsulation and hydrogel microtip fabrication. We demonstrated PEGDA to be a feasible protein entrapment and sensor matrix at the end of an optical fiber. The facile fabrication scheme enabled the control of the size and physical properties of the protein doped hydrogel microtip at the distal end of the optical fiber.

Here, we successfully encapsulated and coupled one of the most commonly used genetically encoded fluorescent protein, GCaMP3 to a physical optical sensor. Up to now, GCaMP3 protein has been only used for imaging purposes. With this study, we extend the use of genetically encoded protein biosensors and develop a universal method for future biosensor applications. The selectivity and sensitivity of sensors is still limited to protein biosensor used. These constraints can be overcome as genetically encoded protein biosensors continue to grow and be engineered to be more sensitive and selective. In this way, protein biosensors would even replace the small molecule dyes in physical sensor applications in the future. The method developed here can also be used for high-throughput monitoring of cellular metabolites. This can be achieved by patterning photocurable material with protein biosensors on glass slides. In similar

manner, optical sensor approach developed here can be adapted to a wireless sensor by replacing the fiber optic spectrometer with proper microelectronics and wireless sensor networks. This approach opens a new design for implantable optical sensors.

## ASSOCIATED CONTENT

### Supporting Information.

The Supporting Information is available free of charge on the ACS Publications website. The following files are available free of charge.

Figure S1. Fabrication schematic of hydrogel discs for swelling experiments.

Figure S2. Microtip fabrication setup

Figure S3. Microtip sensor characterization setup.

Figure S4a. Image of PEG hydrogels prepared in cuvettes.

Figure S4b. Sensor normalized calcium response with respect to the amount of protein inside hydrogel matrix

Figure S5. The representative cryo-SEM images of hydrogel microtips with increasing PEG molecular weight.

Figure S6. The representative cryo-SEM images of hydrogel microtips with increasing monomer concentration.

Figure S7. Performance of microtip sensors grown with varying concentrations of $PEG_{740}DA$.

Table S1. Performance of microtip sensors grown with varying laser power.

Video S1. Microtip sensor growth at the distal end of multimode optical fiber.

## AUTHOR INFORMATION

### Corresponding Author

*(J.L.R.) email: rickus@purdue.edu

ORCID

Jenna L. Rickus: 0000-0002-6325-330X

### Present Addresses

† (R.M.) current affiliation: Intramural Research Program, National Institute on Drug Abuse - National Institutes of Health, Baltimore, MD 21224, USA.

### Notes

The authors declare no competing financial interest.

## ACKNOWLEDGMENT

We are grateful to Jennifer Sturgis and Dr. J. Paul Robinson for their help and support on optical setup. We also would like to thank Dr. Christopher J. Gilpin for his help on SEM measurements.

## REFERENCES

(1) Deuschle, K.; Okumoto, S.; Fehr, M.; Looger, L. L.; Kozhukh, L.; Frommer, W. B. Construction and Optimization of a Family of Genetically Encoded Metabolite Sensors by Semirational Protein Engineering. *Protein Sci.* **2005**, 14, 2304–2314.

(2) Tian, L.; Hires, S. A.; Mao, T.; Huber, D.; Chiappe, M. E.; Chalasani, S. H.; Petreanu, L.; Akerboom, J.; McKinney, S. A.; Schreiter, E. R.; Bargmann, C. I.; Jarayaman V.; Svoboda K.; Looger L.L. Imaging Neural Activity in Worms, Flies and Mice with Improved GCaMP Calcium Indicators. *Nat. Methods* **2009**, 6, 875–881.

(3) Marvin, J. S.; Borghuis, B. G.; Tian, L.; Cichon, J.; Harnett, M. T.; Akerboom, J.; Gordus, A.; Renninger, S. L.; Chen, T.-W.; Bargmann, C. I.; Orger M.B.; Schreiter E.R.; Demb J.B.; Gan W.-B.; Hires S.A.; Looger L.L. An Optimized Fluorescent Probe for Visualizing Glutamate Neurotransmission. *Nat. Methods* **2013**, 10, 162–170.

(4) Dulla, C.; Tani, H.; Okumoto, S.; Frommer, W. B.; Reimer, R. J.; Huguenard, J. R. Imaging of Glutamate in Brain Slices Using FRET Sensors. *J. Neurosci. Methods* **2008**, 168, 306–319.

(5) Looger, L. L.; Lalonde, S.; Frommer, W. B. Genetically Encoded FRET Sensors for Visualizing Metabolites with Subcellular Resolution in Living Cells. *Plant Physiol.* **2005**, 138, 555–557.

(6) Wang, X.-D.; Rabe, K. S.; Ahmed, I.; Niemeyer, C. M. Multifunctional Silica Nanoparticles for Covalent Immobilization of Highly Sensitive Proteins. *Adv. Mater.* **2015**, 27, 7945–7950.

(7) Faccio, G.; Bannwarth, M. B.; Schulenburg, C.; Steffen, V.; Jankowska, D.; Pohl, M.; Rossi, R. M.; Maniura-Weber, K.; Boesel, L. F.; Richter, M. Encapsulation of FRET-Based Glucose and Maltose Biosensors to Develop Functionalized Silica Nanoparticles. *Analyst* **2016**, 141, 3982–3984.

(8) Kim, D.; Herr, A. E. Protein Immobilization Techniques for Microfluidic Assays. *Biomicrofluidics* **2013**, 7, 41501.

(9) Bryant, S. J.; Anseth, K. S. Controlling the Spatial Distribution of ECM Components in Degradable PEG Hydrogels for Tissue Engineering Cartilage. *J. Biomed. Mater. Res. A* **2003**, 64, 70–79.

(10) Rubina, A. Y.; Kolchinsky, A.; Makarov, A. A.; Zasedatelev, A. S. Why 3-D? Gel-Based Microarrays in Proteomics. *Proteomics* **2008**, 8, 817–831.

(11) Kobel, S.; Limacher, M.; Gobaa, S.; Laroche, T.; Lutolf, M. P. Micropatterning of Hydrogels by Soft Embossing. *Langmuir* **2009**, 25, 8774–8779.

(12) Mellott, M. B.; Searcy, K.; Pishko, M. V. Release of Protein From Highly Cross-Linked Hydrogels of Poly(Ethylene Glycol) Diacrylate Fabricated by UV Polymerization. *Biomaterials* **2001**, 22, 929–941.

(13) Kuznetsova, I. M.; Zaslavsky, B. Y.; Breydo, L.; Turoverov, K. K.; Uversky, V. N. Beyond the Excluded Volume Effects: Mechanistic Complexity of the Crowded Milieu. *Molecules* **2015**, 20, 1377–1409.

(14) Dombeck, D. A.; Harvey, C. D.; Tian, L.; Looger, L. L.; Tank, D. W. Functional Imaging of Hippocampal Place Cells at Cellular Resolution During Virtual Navigation. *Nat. Neurosci.* **2010**, 13, 1433–1440.

(15) Grienberger, C.; Konnerth, A. Imaging Calcium in Neurons. *Neuron* **2012**, *73*, 862–885.

(16) McGuigan, J. A.; Lüthi, D.; Buri, A. Calcium Buffer Solutions and How to Make Them: a Do It Yourself Guide. *Can. J. Physiol. Pharmacol.* **1991**, 69, 1733–1749.

(17) Bers, D. M.; Patton, C. W. A Practical Guide to the Preparation of Ca2+ Buffers. *Methods Cell Biol.* **2010**, 99,1-26.

(18) Flory, P. J.; Rehner, J. Statistical Mechanics of Cross-Linked Polymer Networks II. Swelling. *J. Chem. Phys.* **1943**, 11, 521–526.

(19) Canal, T.; Peppas, N. A. Correlation Between Mesh Size and Equilibrium Degree of Swelling of Polymeric Networks. *J. Biomed. Mater. Res.* **1989**, 23, 1183–1193.
(20) Sensi, S. L.; Canzoniero, L. M.; Yu, S. P.; Ying, H. S.; Koh, J. Y.; Kerchner, G. A.; Choi, D. W. Measurement of Intracellular Free Zinc in Living Cortical Neurons: Routes of Entry. *J. Neurosci.* **1997**, 17, 9554–9564.
(21) Hsu, M.-Y.; Hung, Y.-C.; Hwang, D.-K.; Lin, S.-C.; Lin, K.-H.; Wang, C.-Y.; Choi, H.-Y.; Wang, Y.-P.; Cheng, C.-M. Detection of Aqueous VEGF Concentrations Before and After Intravitreal Injection of Anti-VEGF Antibody Using Low-Volume Sampling Paper-Based ELISA. *Sci. Rep.* **2016**, 6, 34631.
(22) Lin, C.-C.; Sawicki, S. M.; Metters, A. T. Free-Radical-Mediated Protein Inactivation and Recovery During Protein Photoencapsulation. *Biomacromolecules* **2008**, 9, 75–83.
(23) Choi, M.; Choi, J. W.; Kim, S.; Nizamoglu, S.; Hahn, S. K.; Yun, S. H. Light-Guiding Hydrogels for Cell-Based Sensing and Optogenetic Synthesis in Vivo. *Nat. Photonics* **2013**, 7, 987–994.
(24) Uranga, J.; Mujika, J. I.; Matxain, J. M. ·OH Oxidation Toward S- and OH-Containing Amino Acids. *J. Phys. Chem. B* **2015**, 119, 15430–15442.
(25) Guo, Y.; Yuan, H.; Rice, W. L.; Kumar, A. T. N.; Goergen, C. J.; Jokivarsi, K.; Josephson, L. The PEG-Fluorochrome Shielding Approach for Targeted Probe Design. *J. Am. Chem. Soc.* **2012**, 134, 19338–19341.
(26) Chatani, S.; Kloxin, C. J.; Bowman, C. N. The Power of Light in Polymer Science: Photochemical Processes to Manipulate Polymer Formation, Structure, and Properties. *Polym. Chem.* **2014**, 5, 2187–2201.
(27) Gu, F.; Neufeld, R.; Amsden, B. Maintenance of Vascular Endothelial Growth Factor and Potentially Other Therapeutic Proteins Bioactivity During a Photo-Initiated Free Radical Cross-Linking Reaction Forming Biodegradable Elastomers. *Eur. J. Pharm. Biopharm.* **2007**, 66, 21–27.
(28) Vitagliano, V.; D'Errico, G.; Ortona, O. In *Encyclopaedia of Surface and Colloid Science*; Hubbard, A. T., Ed.; Marcel Dekker, New York, 2002; pp 4105-4123.
(29) Jradi, S.; Soppera, O.; Lougnot, D. J.; Bachelot, R.; Royer, P. Tailoring the Geometry of Polymer Tips on the End of Optical Fibers via Control of Physico-Chemical Parameters. *Opt. Mater.* **2009**, 31, 640–646.
(30) Soppera, O.; Jradi, S.; Lougnot, D. J. Photopolymerization with Microscale Resolution: Influence of the Physico□Chemical and Photonic Parameters. *J. Polym. Sci., Part A: Polym. Chem.* **2008**, 46, 3783–3794.
(31) Kostov, Y.; Smith, D. S.; Tolosa, L.; Rao, G.; Gryczynski, I.; Gryczynski, Z.; Malicka, J.; Lakowicz, J. R. Directional Surface Plasmon-Coupled Emission From a 3 Nm Green Fluorescent Protein Monolayer. *Biotechnol. Prog.* **2005**, 21, 1731–1735.
(32) Sheng Lin-Gibson; Ronald L Jones; Newell R Washburn, A.; Horkay, F. Structure−Property Relationships of Photopolymerizable Poly(Ethylene Glycol) Dimethacrylate Hydrogels. *Macromolecules* **2005**, 38, 2897–2902.
(33) and, S. L.; Anseth, K. S. Release Behavior of High Molecular Weight Solutes From Poly(Ethylene Glycol)-Based Degradable Networks. *Macromolecules* **2000**, 33, 2509–2515.
(34) Lee, A. G.; Arena, C. P.; Beebe, D. J.; Palecek, S. P. Development of Macroporous Poly(Ethylene Glycol) Hydrogel Arrays Within Microfluidic Channels. *Biomacromolecules* **2010**, 11, 3316–3324.

(35) Reid, B.; Gibson, M.; Singh, A.; Taube, J.; Furlong, C.; Murcia, M.; Elisseeff, J. PEG Hydrogel Degradation and the Role of the Surrounding Tissue Environment. *J. Tissue Eng. Regen. Med.* **2015**, 9, 315–318.

(36) Song, L.; Hennink, E. J.; Young, I. T.; Tanke, H. J. Photobleaching Kinetics of Fluorescein in Quantitative Fluorescence Microscopy. *Biophys. J.* **1995**, 68, 2588–2600.

(37) Badura, A.; Sun, X. R.; Giovannucci, A.; Lynch, L. A.; Wang, S. S. H. Fast Calcium Sensor Proteins for Monitoring Neural Activity. *Neurophotonics* **2014**, 1, 025008–025008.

(38) Kim, H. M.; Jung, C.; Kim, B. R.; Jung, S. Y.; Hong, J. H.; Ko, Y. G.; Lee, K. J.; Cho, B. R. Environment□Sensitive Two□Photon Probe for Intracellular Free Magnesium Ions in Live Tissue. *Angew. Chem., Int. Ed.* **2007**, 46, 3460–3463.

(39) Krezel, A.; Maret, W. Zinc-Buffering Capacity of a Eukaryotic Cell at Physiological pZn. *J. Biol. Inorg. Chem.* **2006**, 11, 1049–1062.

(40) Warren, J. T.; Guo, Q.; Tang, W.-J. A 1.3-Å Structure of Zinc-Bound N-Terminal Domain of Calmodulin Elucidates Potential Early Ion-Binding Step. *J. Mol. Biol.* **2007**, 374, 517–527.

(41) Martin, S. R.; Masino, L.; Bayley, P. M. Enhancement by Mg2+ of Domain Specificity in Ca2+-Dependent Interactions of Calmodulin with Target Sequences. *Protein Sci.* **2000**, 9, 2477–2488.

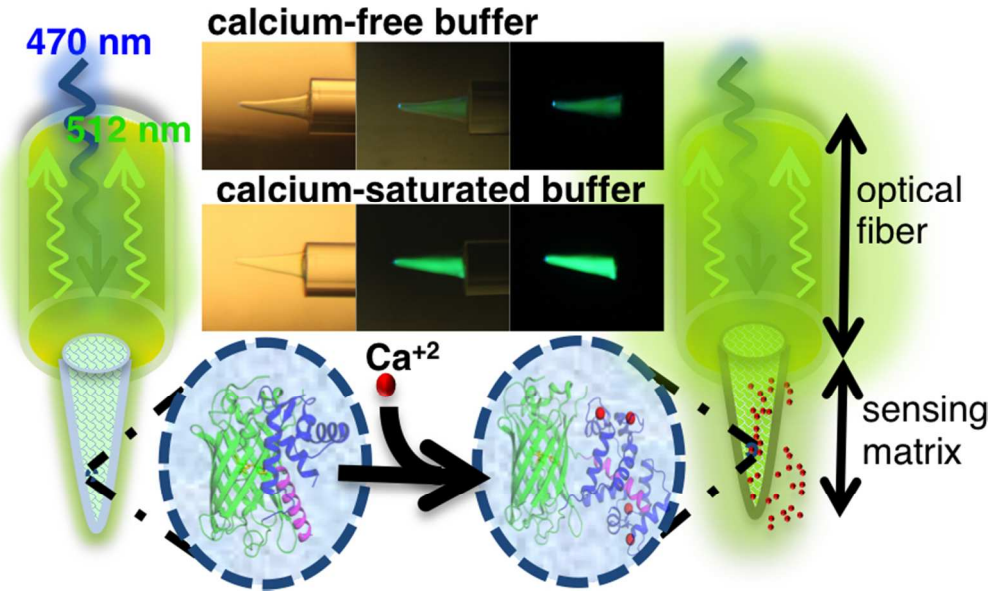


abstract figure

76x44mm (300 x 300 DPI)

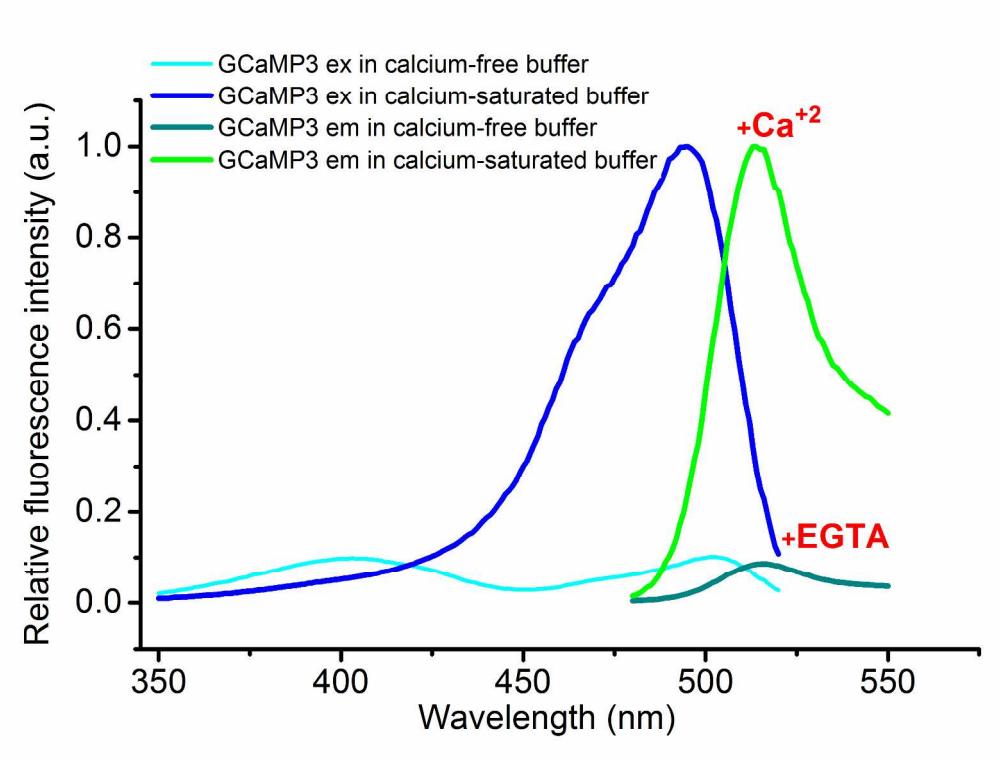


Fluorescence spectra of GCaMP3 in the absence and presence (39 μM) of calcium in MOPS buffer. The fluorescence intensity of each measurement was normalized to the peak of calcium saturated spectrum. The cyan and blue colored lines indicate GCaMP3 excitation spectrum in calcium-free buffer and in calcium-saturated buffer while dark cyan and green colored lines show GCaMP3 emission spectrum in calcium-free buffer and in calcium-saturated buffer, respectively.

272x208mm (300 x 300 DPI)

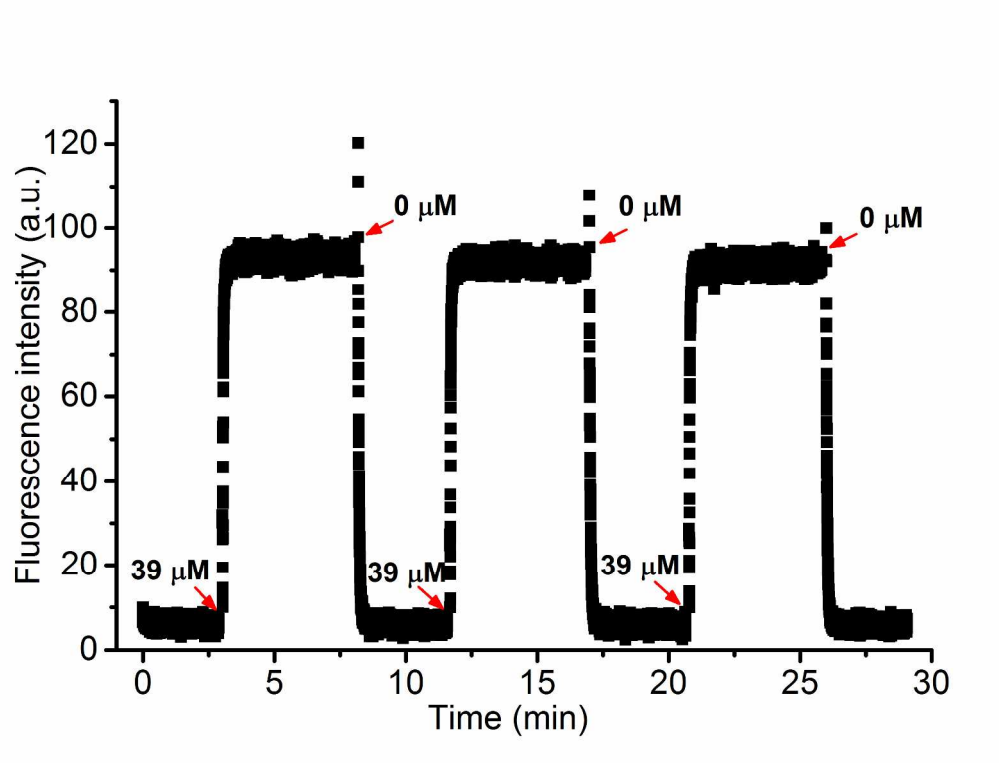


Microtip sensor signal was highly reversible. Arrows show the time points at which the calcium-free buffer was switched to the corresponding concentration on the figure.

272x208mm (300 x 300 DPI)